Metal internalisation by bacterial cells depends on metal biotoxicity and metal to biomass ratio.

Title: Metal internalisation by bacterial cells depends on metal biotoxicity and metal to biomass ratio.

Author: Lili Liang[1], Bryne T. Ngwenya[2]

Author address:

[1]School of Environmental Studies, University of Geoscience, Wuhan, 430074, China.

[2]School of Geosciences, University of Edinburgh, James Hutton Road, Edinburgh EH9 3FE, United Kindom.

Corresponding author: *Lili Liang and Bryne T. Ngwenya*

E-mail:

Lili Liang: lianglily99@126.com

Bryne T. Ngwenya: Bryne.Ngwenya@ed.ac.uk

Metal internalisation by bacterial cells depends on metal biotoxicity and metal to biomass ratio

Lili Liang[1]* *and Bryne T. Ngwenya*[2]*

[1]School of Environmental Studies, University of Geoscience, Wuhan, 430074, China.

[2]School of Geosciences, University of Edinburgh, James Hutton Road, Edinburgh EH9 3FE, United Kindom.

* Corresponding author.

Abstract

The traditional view of metal adsorption to bacterial surfaces is that it can act as a protective mechanism by externalizing the metal outside the cell. However, numerous studies focussing on the biodynamics of metal uptake using biotic ligand models consider metal adsorption to cell surfaces as an important first step in metal uptake and internalisation. In order to resolve these conflicting views, we adsorbed two metals (copper and cadmium) with contrasting metal biotoxicity on *E. coli JM109*, and quantified the distribution of each metal amongst surface sites, periplasmic space and the cytoplasm. Distribution of each metal depended on biotoxicity and metal to biomass ratio. For both metals, low metal to biomass ratio led to most of the metal being associated with the periplasmic space, with less Cd being taken up by cells overall. At high metal to biomass ratios, most of the Cd was associated with surface sites, whereas

Cu also increased in surface sites but remained below periplasmic concentrations. These observations are consistent with metal internalization being the dominant process at low metal to biomass ratios, whereas was active efflux when metal to biomass was high, leading to equilibrium between cytoplasm and surface concentrations. Significantly, efflux was more intense for high biotoxicity Cd, consistent with active enzymatic regulation of Cu internalization/homeastasis, which is essential at low concentrations. Moreover, metal internalization increases as surface-bound metal increases, the maximum being constrained by maximum adsorption consistent with Langmuir adsorption behaviour.

Summarize of paper: Bacterial metal internalisation is a function of metal biotoxicity and metal loading.

Key words: Metal internalisation; Bacteria; Adsorption; Uptake; *E.coli JM109*

1. Introduction

Amongst many geomicrobiologists, the traditional view of metal interaction with bacterial cells is that the metal associates with the cell by biosorption, involving non-specific binding to cell surfaces (Gadd, 2007; Fomina & Gadd, 2014). This has led to a proliferation of studies employing surface complexation models as a basis for

65 developing predictive approaches to quantifying metal uptake, with little to no regard
66 for cellular internalisation of the metal (Fein et al., 1997 & 2001; Ngwenya et al., 2003;
67 Borrok et al., 2005; Tourney et al., 2009; Ngwenya et al., 2010; Kenney and Fein,
68 2011). By integrating biosorption studies with spectroscopic measurements (e.g. infra-
69 red and X-ray absorption spectroscopy), these studies have identified specific
70 functional groups that are responsible for metal complexation at the cell surface,
71 including carboxyl, phosphate, amine, phosphodiester and sulfhydryl moieties.

72 In contrast, there have been numerous and independent studies by biogeochemists
73 focussing on the biodynamics of metal uptake by micro-organisms (including bacteria
74 and algae), in which biosorption is considered only as a first step in metal
75 bioaccumulation, ultimately leading to metal internalisation by cells (Campbell et al.,
76 2002; Duval et al., 2014, 2015, 2016; Rotureau et al., 2015; Present et al., 2017).
77 Building on such approaches, the study by Pabst et al (2010) was one of the first to
78 attempt to quantify metal partitioning between different cellular compartments in a
79 bacterial cell, using selective extraction to demonstrate that cadmium and copper
80 associated differently with the cell surface, periplasm and cytoplasm of the bacteria
81 tested. Specifically, cadmium was mainly found on the surface of the cell, ascribed to
82 an active metal efflux mechanism due to cadmium's toxicity profile. It was thought that
83 the cadmium was bound to the surface functional groups identified from surface
84 complexation models. Such studies provided the platform for recent attempts to
85 combine surface complexation, initial bulk metal concentration and biotic ligand

86 models (BLM), providing a means to predict metal toxicity purely from surface
87 complexation models (Flynn et al., 2014; Duval et al., 2015; Fein, 2017).

88 The aim of this study was to probe deeper into the mechanism behind differences
89 in metal compartmentalisation linked to the biotoxicity profile of the metal. We used
90 the same metals (copper and cadmium) as Pabst et al (2010) but on a different
91 bacterium, *E. coli* JM109. We specifically sought to vary metal to biomass ratio,
92 hypothesising that active metal efflux processes would only be triggered above certain
93 concentration thresholds with little or no control from surface chemistry, as suggested
94 by Pabst et al (2010).

95 ## 2. Materials and methods

96 **2.1 Cell growth and preservations**:

97 Experimental batches of *E.coli* JM109 were grown from the primary culture
98 (stocks) by first plating them overnight in nutrient agar, transferring and growing a
99 single colony overnight in 100ml nutrient broth No.3, and using the overnight culture
100 to inoculate 2L Pyrex flasks containing 1 litre of nutrient broth No.3. Cultures were
101 incubated on a shaker for 48 h at 30 °C. Cells were harvested by centrifugation at
102 11000g for 10 min at 4 °C. The harvested cells were then washed three times in 18 MΩ
103 ultrapure water, freeze-dried and homogenised into powder for use in the experiments
104 described below. Previous studies have shown that most of the cells prepared and
105 preserved by this method are intact and viable (Ngwenya et al., 2003).

2.2 **Metal exposure solutions**

The metal solutions were prepared in 20mL Teflon centrifuge tubes at concentrations ranging from 0.5 to 10 mg/L (0.008 to 0.16mM) of free Cu^{2+} ions using $Cu(NO3)_2$,and Cd from 0.5 to 10mg/L (0.004 to 0.1mM) of Cd^{2+} using $Cd(NO3)_2$ in a inert background electrolyte of 0.01M NaNO3, chosen to limit solution complexation of the metals. This means that although cells were viable (Ngwenya et al., 2003), they were not metabolising. This need not necessarily curtail active enzymatic responses, as shown by previous studies where inert exposure media have been used (e.g. Smeijan et al., 2000). The pH in each tube was adjusted to 5, and geochemical modelling using Visual Minteq showed that both metals were in free ionic form at this pH, and that over 90% each metal is adsorbed to cells at pH 5 (Parker et al., 1995; Ngwenya et al., 2010).

2.3 **Metal adsorption experiments**

Adsorption experiments were conducted at two different cell (biomass) suspension concentrations, 0.5g/L and 2g/L, in order to compare the effect of different metal to biomass ratios, by suspending 10mg and 40mg of freeze-dried bacteria in 20mL of the metal solution. Experiments were performed in triplicate. Tubes were mixed on a carousel at 25±1°C for 30min and then centrifuged to pellet the cells and obtain a supernatant. Previous studies (Wu et al., 2009; Langley and Beveridge, 1999; pabst et al., 2010) and in our laboratory (Ngwenya et al., 2003) have shown that this contact time is sufficient for adsorption to reach equilibrium. Chemical buffering agents were not added during the whole procedure, and pH was maintained throughout the study to

within 0.2pH units. Following equilibration, cells were separated from the supernatant by centrifugation at 11000g for 10 min at 4 °C. The cell pellet was used for compartmentalisation experiments described below. The supernatant was filtered, acidified to 2% v/v with nitric acid, and analyzed for Cu or Cd using Inductively Coupled Plasma-Optical Emission Spectrometry (ICP-OES, PerkinElmer 5300DV). Analytical quality on the ICP-OES was checked against a certified mixed metal standard (M6, Merck), yielding precision better than 2% relative standard deviation and accuracy to within 1% of the certified values.

2.4 Characterization of metal-cell compartmentalization

We adopted the method of Pabst et al (2010) and Mclean et al (2013), but with slight modifications, to determine metal-cell compartmentalization following adsorption by measuring the proportion of Cu and Cd associated with surface exchange sites (q_{exch}), the periplasmic space (q_{peri}) and the cytoplasm (q_{cyt}). Metal associated with exchange sites on the cell surface were extracted by suspending the cell pellet into 20mL of 5mM Ca^{2+} as $Ca(NO_3)_2$ which had been adjusted to pH 5 on a carousel at 25±1°C for 20min (salt et al., 1997). The suspension was centrifuged at 11000g at 4℃ and the supernatant analyzed for the desorbed metal. The step for determining outer membrane and periplasmic metal compartmentalization was modified by increasing the extraction time in 20ml of 20 mM EDTA (adjusted to pH 5) from 20s (Pabst et al., 2010) to 20 minutes to allow longer equilibration. This is because most bacterial cells contain a certain amount of EPS, and since EDTA is one of the reagents used to disrupt EPS

148 (Liu et al. 2002; Tourney et al., 2008; D'Abzac et al., 2010), we assumed that this step
149 should also extract metal bound to EPS but not exchanged with Ca in the first step,
150 allowing for the fact that metal movement/extraction from EPS can be affected by slow
151 diffusion (Ha et al., 2010). After centrifugation, the remaining pellet was digested with
152 3mL concentrated nitric acid, heated to 120℃ for 5min, then dried and re-dissolved in
153 20 ml of 2% HNO3 for ICP-OES analysis. The sum of Cu and Cd from the three
154 extraction steps was designated as the total amount of metal associated with the cell,
155 q_{frac}. Data quality was checked by mass balance calculations of the three
156 compartments, which was between 90% and 110% when the initial adsorbed
157 concentration and the sum of extracted metals were compared.

158 **2.5 Acid-base titrations and surface complexation modelling**

159 Potentiometric titrations were performed on suspensions of each bacteria
160 following the protocol of Ngwenya et al (2003) in order to characterize the number and
161 types of proton-active functional groups present on cell surfaces. Briefly, titrations were
162 carried out at room temperature on 50-ml suspensions of the bacteria in a background
163 electrolyte of 0.01M $NaNO_3$, which had been purged of dissolved gases with O_2- and
164 CO_2-free N_2 for 30 minutes. Titrations were conducted using an automated DL53
165 (Mettler Toledo) burette assembly using 0.1M NaOH following acidification of the
166 suspension to pH ~3. The titrant was standardised in triplicate against potassium
167 hydrogen pthalate (KHP) and the mean concentration of the three standards used in the
168 calculations. The titrations were carried out in polypropylene beakers sealed to

atmospheric gases and a positive N_2 pressure was maintained throughout the titration. The titrator was programmed in dynamic mode and successive titrant additions were made only when a stability of 0.1mV/s had been attained. Base consumption data in the form of H^+ adsorbed was normalised to the dry mass concentration of bacteria (10g/L) and modelled using FITEQL4 (Herbelin & Westall, 1999) to calculate deprotonation constants and surface densities of proton-active sites.

2.6 Fourier Transform Infrared Spectroscopy

Fourier Transform Infrared (FTIR) spectroscopy was performed on cells before and after adsorption of 5mg/L of each metal in order to detect functional groups that may contribute to metal binding/adsorption by cells to complement potentiometric titrations. To prepare samples, 0.01g of freeze-dried cells were mixed with 20 ml solutions of 5mg L^{-1} of $Cu(NO_3)_2$ and $Cd(NO_3)_2$ in 0.01M NaNO3 background electrolyte and adjusted to pH 5. Samples were performed in triplicate, and tubes were mixed on a carousel at 25±1°C for 30min, then centrifuged to pellet and the pellet freeze-dried. The prepared samples, together with controls (freeze-dired cells without metal adsorption) were mixed with KBr in the ratio of 1:100 and pellets of 13mm diameter were prepared at 8×10^3 $kgcm^2$ pressure. The IR spectra were carried out on a Nicolet 6700 (Thermo Scientific, USA) spectrometer over the wave number range of 400-4000 cm^{-1}. For each sample, 40 scans were collected at a resolution of 0.09 cm^{-1} and spectra added.

2.7 Data analysis.

190 The amount of metal adsorbed (qads, mmol/kg) for each initial metal
191 concentration was calculated by difference between initial and equilibrium metal
192 concentration (Ce, mmol/L). Since pH was maintained constant within experimental
193 limits, data was analyzed in the form of pH isotherms where bulk adsorbed (qads) and
194 compartmentalised (q_{exch}, q_{peri}, and q_{cyt}) metal contents were plotted against equilibrium
195 metal concentrations in solution (Figure 1). In this form, adsorption displayed linear
196 behaviour when metals were equilibrated with 2g/L cell suspensions, leading to pseudo-
197 linear distribution coefficients (Figure 1A and 1B)). For 0.5g/l cell suspensions, the
198 relationships were non-linear and hence a one site Langmuir model was used to
199 compare parameters for the distribution of metal adsorption to cells (Figure 1C and 1D.
200 The Langmuir model is given in equation 1 and relates the amount of metal adsorbed
201 (q) in mmol·kg^{-1} and the concentration of the metal in solution at equilibrium:

202 $$q = \frac{Q^0 b C_{eq}}{1 + b C_{eq}}$$

203 where Q^0 is the maximum mass adsorbed at saturation conditions per mass unit of
204 adsorbent (mmol·kg^{-1}), and b is an empirical constant with units of inverse
205 concentration (Bubba et., 2003; Mclean et al., 2013).

206

207 # 3. Results and discussion

208 ## 3.1 Metal adsorption and compartmentalization.

209 Bulk adsorption isotherms for the two metals and at different metal to biomass
210 ratios were presented Figure 1, which also plots the sum of fractionated metal (qfrac)
211 against bulk equilibrium concentrations and associated fitted parameter were presented
212 Table 1 and 2. Whilst this is not evidence that the extraction steps are uniquely selective
213 to the specific compartments, the data clearly shows that the extractions are quantitative
214 and robust, being within experimental/analytical error.

215 For the fractionated data, we noted differences in the behavior of copper and
216 cadmium, as well as in the metal uptake behavior that depended on the amount of cells
217 equilibrated with the same initial metal solution concentrations. Consequently, we
218 describe copper and cadmium results separately, by comparing/contrasting cell to
219 biomass ratio, with lower concentrations defined as those with low metal to biomass
220 ratio.

221 **3.1.1 Copper.**

222 At low metal to bacteria ratios (2g/L cells), copper isotherms are nearly linear
223 (Figure 2A,). Most of the Cu resides in the EDTA-extractable fraction, considered to
224 represent Cu bound to periplasmic space and the concentration in this fraction increases
225 steeply with external (equilibrium) copper concentration. Surface adsorption (qexch)
226 represents the lowest fraction in both types of cells and this fraction is only weakly
227 dependent on external copper concentrations.

228 At high metal to biomass ratios (0.5g/L bacteria), the adsorption isotherms are
229 non-linear and all individual compartments display Langmuir behaviour (Figure 2C,),

consistent with a limiting uptake value as concentrations in solution increase. However, the highest concentrations still occur in the EDTA-extractable fraction (periplasmic space), particularly at low equilibrium concentrations (Table 1). In addition, the exchangeable fraction is now a significant proportion of the total Cu uptake whereas the cytoplasmic fraction remains fairly low, overtaking the periplasmic fraction only at high equilibrium concentrations, although data at high equilibrium concentrations is limited. Such an observation is similar to that of Pabst et al (2010) who reported that for the KT2440 pseudomonad, more copper was associated with the periplasmic space at low equilibrium solution concentrations whereas the proportion of Cu on the surface increased relative to that in the periplasm with increasing solution concentration.

Thermodynamic models of metal uptake by cells, such as the Free Ion activity Model (FIAM, Morel, 1983) and the Biotic Ligand Model (BLM,) are predicted on the assumption that metal internalisation rate is dependent on the concentration of the free metal in the fluid (for FIAM) or metal adsorbed on the surface (BLM). Observations generally support these assumptions but especially so when the metal concentration in solution is low (Smiejan et al., 2003). In such low metal to biomass case, the metal efflux rate is negligible with respect to the internalization rate (essentially no active regulation), which may explain the linear dependence of copper internalisation on solution concentration (Figure 2A).

However, copper is also a micronutrient that is required at low concentrations as a co-factor in multiple proteins where it participates in a range of redox reactions

(Tavares et al., 2006; Arguello et al., 2013), although it can also be toxic at high concentrations (Rosenzweig, 2001). Its uptake and cellular concentration is therefore closely regulated by a range of so-called metallochaperone proteins that collect/deliver copper ions from/to specific transport P-type ATPases with high copper binding affinities (Rosenzwieg, 2001; González-Guerrero et al., 2008). Although cells were not metabolically active (but viable) in our experiments, the observation that most copper is concentrated in the periplasm at low (equilibrium) concentrations and high cell concentrations is entirely consistent with an active uptake mechanism designed to accumulate essential levels of copper. As relative solution concentrations increase, however, the same active mechanisms will operate to reverse uptake by effluxing copper to the external surface where passive biosorption (exchangeable) processes operate. This switch is clearly evident in our low biomass data, (Figure 2C), and such active regulation could explain the relatively low and nearly constant copper concentration in the cytoplasmic space.

Against this argument is the observation that at the end of the adsorption experiment, cells showed light blue pigmentation consistent with copper being in the divalent state. Studies have shown that copper is chaperoned into/out of cells in monovalent (Cu^{+}) state (Pufahl et al., 1997; Rosenzweig, 2001), so the blue colour would contradict active regulation. It is conceivable that the blue colour represents only the exchangeable component, especially as this was more evident in experiments with low bacterial biomass where the exchangeable fraction was indeed high.

3.1.2 Cadmium

The behaviour of Cd at low metal to bacteria ratios is similar to that of copper in that most of the Cd resides in the EDTA-extractable fraction (periplasmic space). However, there are also subtle differences between Cd and Cu (Figure 2B). Firstly, significantly less Cd is taken up by cells compared to copper, although this could simply reflect the lower (in mole terms) total cadmium present compared to copper. Secondly, similar levels of Cd were found in exchangeable sites and in the cytoplasm at low equilibrium concentrations but the exchangeable fraction increases steeply above cytoplasmic contents at high equilibrium concentrations. The biggest difference from copper was observed for experiments using low bacteria concentrations (0.5g/L), where we measured a complete reversal in the compartmentalization of Cd between periplasmic space and exchangeable sites across all equilibrium concentrations (Figure 2D, Table 2).

As with copper, the relative partitioning of cadmium at low equilibrium concentrations is consistent with passive uptake. Unlike copper, however, cadmium is not an essential micronutrient and is extremely toxic to microorganisms, partly by interfering with cellular homeostasis of essential transition metals such as zinc (e.g. Ammendola et al., 2014). A study of Cd uptake by Smijean et al (2003) showed that the bacterium *Rhodospirillum rubrum* responded to high Cd concentrations by actively transporting internalized Cd to the outside of the cell, as well as secreting an exudate that was able to complex Cd in solution, thereby reducing both internalized and

293 adsorbed Cd (Mirimanoff & Wilkinson, 2000). Our data at high solution concentrations
294 is consistent with such active Cd regulation, except that in our case, the externalized Cd
295 is trafficked to exchangeable sites (Figure 2D).

296 **3.1.3 Metal efflux leads to equilibration between surface sites and cytoplasm at**
297 **high surface loading**

298 The analysis of metal partitioning from empirical equilibrium adsorption models
299 (e.g. Langmuir) as in this study does not lend itself to evaluation of metal uptake
300 biodynamics (internalization and efflux rates, affinity constants etc.) to enable a robust
301 inference of the relationship between metal internalization/toxicity and the
302 concentration of metal bound at the surface/transport sites (as required for example by
303 the biotic ligand model). Establishing such relationships is necessary because current
304 understanding of metal uptake dynamics assumes rapid equilibration between bulk
305 solution and surface sites, with metal internalization being the rate-limiting process
306 (Kola & Wilkinson, 2005); thus toxicity depends on the amount of metal bound on
307 surface sites (Flynn & Fein, 2014). In order to provide further insight into the
308 relationship between metal internalization and surface-site loading, we plotted
309 internalized concentrations (qcyt) against (qexch + qperi), the latter assumed to
310 represent surface-bound metal concentration (note that plotting against qexch only also
311 gives similar relationships) that is in equilibrium with solution concentration (Figure 3).

312 As in Figure 3, there is a clear difference in behavior between high and low metal
313 to biomass treatments. For high metal to biomass conditions (Figure A and B), the data

314 fits a straight line. In contrast, systems with low metal to biomass ratios are non-linear,
315 with steep slopes at low surface metal loadings that evolve to constant slopes with
316 increasing surface metal loading (Figure 3C and D).

317 A plausible interpretation of these differences/relationships is that they relate to the
318 balance between internalization and efflux rates, since these vary with metal
319 concentration/surface loading (Kola et al., 2005; Paquet et al., 2015). To illustrate this,
320 we can define the internalization rate ($J_{int,}$ mmolkg^{-1}s^{-1}) with respect to this fraction as:

321 $$J_{int} = k_{int}(q_{exch} + q_{per}) \quad (2)$$

322 where k_{int} is the first order internalization rate constant (s^{-1}). Similarly, the efflux rate
323 ($J_{effl,}$ mmolkg^{-1}s^{-1}) can be defined with respect to the metal concentration in the
324 cytoplasm (qcyt), thus:

325 $$J_{effl} = k_{effl}q_{cyt} \quad (3)$$

326 where k_{effl} is the first order efflux constant (s^{-1}). Since the surface is equilibrated with
327 the solution at sampling and total metal adsorbed is time-invariant, a reasonable
328 approximation is to assume that the surface-bound metal is also in equilibrium (or at
329 least in steady-state) with the internalized metal (qcyt), at least over short time scales
330 (In reality, qcyt changes with time, often increasing during early exposure times
331 followed by subsequent decreases as efflux kicks in (e.g. Mairmanoff & Wlkinson,
332 2000; Smeijan et al., 2003)). Under such conditions and assuming these are single step

333 (elementary reactions), we can invoke microscopic reversibility (Stumm & Morgan,
334 1996) and equate the internalization rate to the efflux rate, thus:

335 $$k_{int}\left(q_{exch} + q_{per}\right) = k_{efflux} q_{cyt} \quad (4)$$

336 such that

337 $$q_{cyt} = \frac{k_{int}}{k_{efflux}}\left(q_{exch} + q_{per}\right) \quad (5)$$

338 Figure 3 is, in fact a plot of equation (5), where k_{int}/k_{efflux} is the slope of the lines/curves.
339 For high metal to biomass ratio, the straight-line relationship means that this slope can
340 be considered as equilibrium constant (*K*), and partly validates our initial assumption
341 above, since:

342 $$\frac{q_{cyt}}{q_{exch}+q_{per}} = \frac{k_{int}}{k_{efflux}} = K \quad (6)$$

343 This is a new finding that needs to be checked against further experimental data but the
344 low values of *K* are indicative of the dominance of metal efflux rates when cells are
345 exposed to high metal concentrations. *K* values for Cu (0.053?) and Cd (0.064) are equal
346 within the noise of the data, possibly because both metals are being actively effluxed at
347 these high concentrations whereas because equation (5) assumes purely a passive
348 equilibrium process. Significantly, the linear relationship also implies that metal
349 internalization can increase beyond cellular capacity to detoxify the metal through
350 active efflux, eventually poisoning the cell, although the observed Langmuir uptake
351 means that qexch (and qperi) is constrained by the concentration of organic ligands on
352 the surface. In contrast, it was clear in Figure 2 that Cd was severely effluxed to

353 exchangeable sites at these high concentrations; the most likely cause of which is active
354 regulation. For systems with low metal to biomass ratios, internalization dominates at
355 low surface loadings (large *K*), eventually switching to efflux dominance as surface
356 loading increases (Figure 3C and D). This is entirely consistent with previous studies
357 (e.g. Smeijan et al., 2003; Kola et al., 2005; Paquet et al., 2015).

358 **3.1.4 Surface site ligands responsible for metal binding.**

359 Another possible explanation for the differences between low and high metal to
360 biomass loading may be the identity of surface active ligands present on cell surfaces
361 that are involved in metal binding. In particular, a number of studies have shown that
362 metal ions preferentially bind to sulfhydryl (-S-H) groups on bacterial cell surfaces at
363 low metal to biomass ratios, with other ligands (notably carboxyl, phosphate and amine
364 functional groups) becoming important only at high metal to biomass ratios (Mishra et
365 al., 2010; Yu and Fein, 2015; Nell and Fein, 2017). Consequently, we determined the
366 identity of surface ligands on *E. coli* cells by performing surface complexation
367 modelling of potentiometric (proton adsorption) titration data, along with infrared
368 spectroscopy.

369 We modelled proton binding data to 10g/L suspensions of the bacteria (data not
370 shown) using FITEQL4 (Herbelin et al., 1999) to calculate protonation constants and
371 surface site concentrations of surface ligands (Table 3) that can contribute to metal
372 adsorption on cell surfaces. Consistent with previous studies (Borrok et al., 2005; Fein
373 et al., 2005; Tourney et al., 2008; Pabst et al., 2010), the best-fitting model consisted of

four discrete proton active sites, with *p*Ka values of 3.48, 5.47, 7.34 and 9.97 and with cell densities of 6.25, 4.39, 1.56, 3.86 x 10^{-4} mol/Kg. These protonation constants are generally ascribed to phosphodiester, carboxyl, phosphate and amine/hydroxyl ligands. Surfhydryl groups are generally thought to be too low to be detectable by this technique other through selective thiol blocking (Yu et al., 2014), but some studies have reported them using Infrared (Batool et al., 2014) and Raman (Culha et al., 2008) spectroscopy. We did not detect sulfhydryl groups on cells of *E. coli JM109* in our study, evidenced by the absence of peaks in the 2300-2500 cm^{-1} region (Battol et al., 2014) in Figure 4. By contrast, vibrations due to amide (1500-1800 cm^{-1}), carboxyl (~1400 cm^{-1}), phosphate (1240, 1085 cm^{-1}), and hydroxyl (~3448 cm^{-1}) groups are present, and their intensities decrease significantly following contact with Cu and Cd. Thus, while we can't completely rule out metal binding to sulfhydryl groups in our study, most of the metal is likely to be bound to non-sulfur ligands, particularly given that the initial metal concentrations (> 5 μmol/L) are well above those at which sulfhydryl adsorption dominates (Yu and Fein, 2015). We regard this as further evidence that metal internalisation depend on differences in metal to biomass ratio and active regulation that depends on the biotoxicity of the metal, other than differences in which ligands are involved in adsorption. Such active regulation is a common feature of viable microbial cells, including algae (e.g. Chen et al., 2010) even when cells are not actively metabolizing.

4. Conclusions

The aim of this study was to characterise metal partitioning in different cellular compartments of E. coli JM109 as a basis for probing the role of metal loading and the biotoxicity of the metal on metal biodynamics. Adsorption was linearly dependent on equilibrium concentrations (linear distribution co-efficient) at low metal to biomass ratio, but showed Langmuir type adsorption isotherms at high metal to biomass ratio. Distribution of each metal amongst surface sites, periplasmic space and cytoplasm depended on metal biotoxicity and metal to biomass ratio. In both cases, low metal to biomass ratio led to most of the metal being associated with the periplasmic space, with less Cd being taken up by cells overall. At high metal loading, most of the Cd was associated with surface sites, whereas Cu also increased in surface sites but remained below periplasmic concentrations. These observations are consistent with metal internalization being only dependent on the concentration of the metal in solution when metal to biomass is low and below toxic concentrations, but active efflux when metal loading is high. Significantly, efflux was more intense for high toxic element (Cd), consistent with active enzymatic regulation of Cu internalization/homeastasis, which is micronutrient element at low concentrations. Metal internalization increases as surface-bound metal increases, the maximum being constrained by maximum adsorption consistent with Langmuir adsorption behaviour. Potentiometric titrations, coupled with infrared spectroscopy the involvement of amide, carboxyl, phosphate and hydroxyl

groups in metal surface adsorption, while sulfhydryl groups were undetectable by both techniques.

Acknowledgments:

We acknowledge the hospitality accorded by the School of GeoSciences during my stay in the University of Edinburgh, and thanks Dr. Lorna Eades for help with ICP-OES analysis. This study was financially by the China Scholarship Council to Lili Liang for a one year visit to the UK(201406415064).

References

Ammendola, S., Cerasi, M., Battistoni, A., 2014. Deregulation of transition metals homeostasis is a key feature of cadmium toxicity in Salmonella. BioMetals, 27(4): 703-714.

434 Argüello, J.M., Raimunda,D., Padilla-Benavides, T., 2013. Mechanisms of copper
435 homeostasis in bacteria. Frontiers in cellular and infection microbiology, 3(73):

436 Batool, R., Yrjala, K., Hasnain, S., 2014. Impact of environmental stress on biochemical
437 parameters of bacteria reducing chromium. Brazilian Journal of Microbiology, 45
438 (2): 573-583.

439 Borrok, D., Turner, B.F., Fein, J.B., 2005. A universal surface complexation framework
440 for modeling proton binding onto bacterial surfaces in geologic settings. American
441 Journal of Science, 305: 826-853.

442 Bubba, M.D., Arias, C.A., Brix, H., 2003. Phosphorus adsorption maximum of sands
443 for use as media in subsurface flow constructed reed beds as measured by the
444 Langmuir isotherm. Water Research, 37(14): 3390-3400.

445 Campbell, P.G.C., Errécalde, O., Fortin, C., Hiriart-Baer, V.P., Vigneault, B., 2002.
446 Metal bioavailability to phytoplankton—applicability of the biotic ligand model.
447 Comparative Biochemistry and Physiology Part C: Toxicology & Pharmacology,
448 133(1): 189-206.

449 Chen, Z., Zhu, L., Wilkinson, K.J., 2010. Validation of the biotic ligand model in metal
450 mixtures: bioaccumulation of lead and copper. Environmental Science &
451 Technology 44: 3580-3586.

452 Culha, M., Adiguzel, A., Yazici, M.M., Kahraman, M., Sahin, F., Gulluce, M., 2008.
453 Characterization of thermophilic bacteria using surface-enhanced Raman
454 scattering. Applied Spectroscopy, 62 (11): 1226-1232.

455 D'Abzac, P., Bordas, F., Van Hullebusch, E., Lens, P.N.L., Guibaud, G., 2010.
456 Extraction of extracellular polymeric substances (EPS) from anaerobic granular
457 sludges: comparison of chemical and physical extraction protocols. Applied
458 Microbiology and Biotechnology, 85(5): 1589-1599.

459 Duval, J.F.L. Rotureau, E., 2014. Dynamics of Metal Uptake by Charged Soft
460 Biointerphases: Impacts of Depletion, Internalisation, Adsorption and Excretion.
461 Physical Chemistry Chemical Physics, 16: 7401-7416.

462 Duval, J.F.L., Paquet, N., Lavoie, M., Fortin, C., 2015. Dynamics of Metal Partitioning
463 at the Cell−Solution Interface:Implications for Toxicity Assessment under
464 Growth-Inhibiting Conditions. Environ. Sciecnce.Technol. 49 (11): 6625–6636.

465 Duval, J.F.L., Présent, R.M., Rotureau, E., 2016. Kinetic and Thermodynamic
466 Determinants of Trace Metal Partitioning at Biointerphases: The Role of
467 Intracellular Speciation Dynamics. Physical Chemistry Chemical Physics, 18:
468 30415-30435.

469 Duval, J.F.L., 2017. Chemodynamics of Metal Ion Complexation by Charged
470 Nanoparticles: A Dimensionless Rationale for Soft, Core-Shell and Hard Particle
471 Types. Physical Chemistry Chemical Physics, 19: 11802-11815.

472 Fein, J.B., 2017. Advanced biotic ligand models: Using surface complexation modeling
473 to quantify metal bioavailability to bacteria in geologic systems. Chemical
474 Geology, 464(Supplement C): 127-136.

475 Fein, J.B., Boily, J.F., Yee, N., Gorman-Lewis, D., Turner, B.F., 2005. Potentiometric
476 titrations of Bacillus subtilis cells to low pH and a comparison of modeling
477 approaches. Geochimica et Cosmochimica Acta, 69(5): 1123-1132.

478 Fein, J.B., Daughney, C.J., Yee, N., Davis, T.A., 1997. A chemical equilibrium model
479 for metal adsorption onto bacterial surfaces. Geochimica et Cosmochimica Acta,
480 61(16): 3319-3328.

481 Fein, J.B., Martin, A.M., Wightman, P.G., 2001. Metal adsorption onto bacterial
482 surfaces: development of a predictive approach. Geochimica et Cosmochimica
483 Acta, 65(23): 4267-4273.

484 Flynn, S.L., Szymanowski, J.E.S., Fein, J.B., 2014. Modeling bacterial metal toxicity
485 using a surface complexation approach. Chemical Geology, 374-375(Supplement
486 C): 110-116.

487 Fomina, M., Gadd, G.M., 2014. Biosorption: current perspectives on concept, definition
488 and application. Bioresource Technology, 160(Supplement C): 3-14.

489 Gadd, G.M., 2007. Geomycology: biogeochemical transformations of rocks, minerals,
490 metals and radionuclides by fungi, bioweathering and bioremediation.
491 Mycological research, 111(1): 3-49.

492 González-Guerrero, M., Eren, E., Rawat, S., Stemmler, T.L., Argüello, J.M., 2008.
493 Structure of the two transmembrane Cu+ transport sites of the Cu+-ATPases.
494 Journal of Biological Chemistry, 283(44): 29753-29759.

495 Ha, J., Gelabert, A., Spormann, A.M., Brown, G.E., 2010. Role of extracellular
496 polymeric substances in metal ion complexation by Shewanella oneidensis: bactch
497 uptake, thermodynamic modelling, ATR-FTIR, and EXAFS study. Geochimica
498 Cosmochimica Acta 74 (1): 1-15.

499 Herbelin, A.L., Westall, J.C., 1999. FITEQL 4.0: a Computer Program for
500 Determination of Chemical Equilibrium Constants from Experimental Data;
501 Report 99–01. Department of Chemistry Oregon State University, Corvallis.

502 Kenney, J.P.L., Fein, J.B., 2011. Importance of extracellular polysaccharides on proton
503 and Cd binding to bacterial biomass: A comparative study. Chemical Geology,
504 286(3–4): 109-117.

505 Kola, H., Wilkinson, K.J., 2005. Cadmium uptake by a green alga can be predicted by
506 equilibrium modelling. Environmental Science & Technology 39: 3040-3047.

507 Langley, S., Beveridge, T.J., 1999. Effect of O-Side-Chain- Lipopolysaccharide
508 Chemistry on Metal Binding. Applied and Environmental Microbiology, 65(2):
509 489-498.

510 Liu, H., Fang, H.H.P., 2002. Extraction of extracellular polymeric substances (EPS) of
511 sludges. Journal of Biotechnology, 95(3): 249-256.

512 McLean, J.E., Pabst, M.W., Miller, C.D., Dimkpa, C.O., Anderson, A.J., 2013. Effect
513 of complexing ligands on the surface adsorption, internalization, and bioresponse
514 of copper and cadmium in a soil bacterium, Pseudomonas putida. Chemosphere,
515 91(3): 374-382.

516 Mirimanoff, N., Wilkinson, J., 2000. Regulation of Zn Accumulation by a Freshwater
517 Gram-Positive Bacterium (Rhodococcus opacus). Environmental science &
518 technology, 34(4): 616-622.

519 Mishra, B., Moyanov, B., Bunker, B.A., Kelly, S.D., Kemmer, K. M., Fein, J. B., 2010.
520 High- and low-affinity binding sites for Cd on the bacterial cell walls of Bacillus
521 subtilis and Shewanella oneidensis. Geochimica Cosmochimica Acta 74 (15):
522 4219-4233

523 Morel, F.M., 1983. Complexation: trace metals and microorganisms. Principles of
524 Aquatic Chemistry. Wiley, New York(1983), pp 300-309.

525 Nell, R.M., Fein, J.B., 2017. Influence of sulfhydryl groups on metal binding to bacteria.
526 Geochimica Cosmochimica Acta 199: 210-221.

527 Ngwenya, B.T., Sutherland, I.W., Kennedy, L., 2003. Comparison of the acid-base
528 behaviour and metal adsorption characteristics of a gram-negative bacterium with
529 other strains. Applied Geochemistry, 18(4): 527-538.

530 Ngwenya, B.T., Magennis, M., Olive, V., Mosselmans, J.F.W., Ellam, R.M., 2010.
531 Discrete Site Surface Complexation Constants for Lanthanide Adsorption to

532 Bacteria As Determined by Experiments and Linear Free Energy Relationships.
533 Environmental Science and Technology, 44(2): 650-656.

534 Pabst, M.W., Miller, C.D., Dimkpa, C.O., Anderson, A.J., McLean, J.E., 2010.
535 Defining the surface adsorption and internalization of copper and cadmium in a
536 soil bacterium, Pseudomonas putida. Chemosphere, 81(7): 904-910.

537 Paquet, N., Lavoie, P., Maloney, F., Duval, J.F.L., Campbell, P.G.C., Fortin., C., 2015.
538 Cadmium Accumulation and Toxicity in the Unicellular Alga Pseudokirchneriella
539 Subcapitata: Influence of Metal-Binding Exudates and Exposure Time.
540 Environmental Toxicology and Chemistry, 34, (7): 1524–1532.

541 Parker, D.R., Norvell, W.A., Chaney, R., 1995. GEOCHEM-PC—a chemical
542 speciation program for IBM and compatible personal computers. Chemical
543 equilibrium and reaction models(chemicalequilib): 253-269.

544 Present, R.M., Rotureau, E., Billard, P., Pagnout, C., Sohm, B., Justine, F., Gley R.,
545 Pinheiro, J.P., Duval J.F.L., 2017. Impact of Intracellular Metallothionein on
546 Metal Biouptake and Partitioning Dynamics at Bacterial Interfaces. Physical
547 Chemistry Chemical Physics 19: 29114-29124.

548 Pufahl, R., Singer, C., Peariso, K., Lin, S.J., Schmidt, P., Fahrni, C., 1997. Metal ion
549 chaperone function of the soluble Cu (I) receptor Atx1. Science, 278(5339): 853-
550 856.

551 Rosenzweig, A.C., 2001. Copper delivery by metallochaperone proteins. Accounts of
552 Chemical Research, 34(2): 119-128.

553 Rotureau, E., Billard, P., Duval, J.F.L., 2015. Evaluation of Metal Biouptake from the
554 Analysis of Bulk Metal Depletion Kinetics at Various Cell Concentrations: Theory
555 and Application. Environmental Science & Technology 49, (2): 990-998.

556 Salt, D.E., Pickering, I.J., Prince, R.C., Gleba, D., Dushenkov, S., Smith, R.D., 1997.
557 Metal Accumulation by Aquacultured Seedlings of Indian Mustard.
558 Environmental Science and Technology, 31(6): 1636-1644.

559 Smiejan, A., Wilkinson, K.J., Rossier, C., 2003. Cd Bioaccumulation by a Freshwater
560 Bacterium, Rhodospirillum rubrum. Environmental science & technology, 37(4):
561 701–706.

562 Stumm, W., Morgan, J.J., 1996. Aquatic Chemistry. John Wiley & Sons, Inc.,
563 Chichester. 1092pp.

564 Tavares, P., Pereira, A.S., Moura, J.J.G., Moura, I., 2006. Metalloenzymes of the
565 denitrification pathway. Journal of Inorganic Biochemistry, 100(12): 2087-2100.

566 Tourney, J., Ngwenya, B.T., Mosselmans, J.W.F., Tetley, L., Cowie, G.L., 2008. The
567 effect of extracellular polymers (EPS) on the proton adsorption characteristics of
568 the thermophile Bacillus licheniformis S-86. Chemical Geology, 247(1): 1-15.

569 Tourney, J., Ngwenya, B.T., 2009. Bacterial extracellular polymeric substances (EPS)
570 mediate CaCO3 morphology and polymorphism. Chemical Geology, 262(3–4):
571 138-146.

572 Wu, S.C., Peng, X.L., Cheung, K.C., Liu, S.L., Wong, M.H., 2009. Adsorption kinetics
573 of Pb and Cd by two plant growth promoting rhizobacteria. Bioresource
574 Technology, 100(20): 4559-4563.

575 Yu, Q., Fein, J.B., 2015. The effect of metal loading on Cd adsorption onto Shewanella
576 oneidensis bacterial cell envelopes: The role of sulfhydrl sites. Geochimica
577 Cosmochimica Acta 167: 1-10.

578
579
580
581
582
583
584
585
586
587

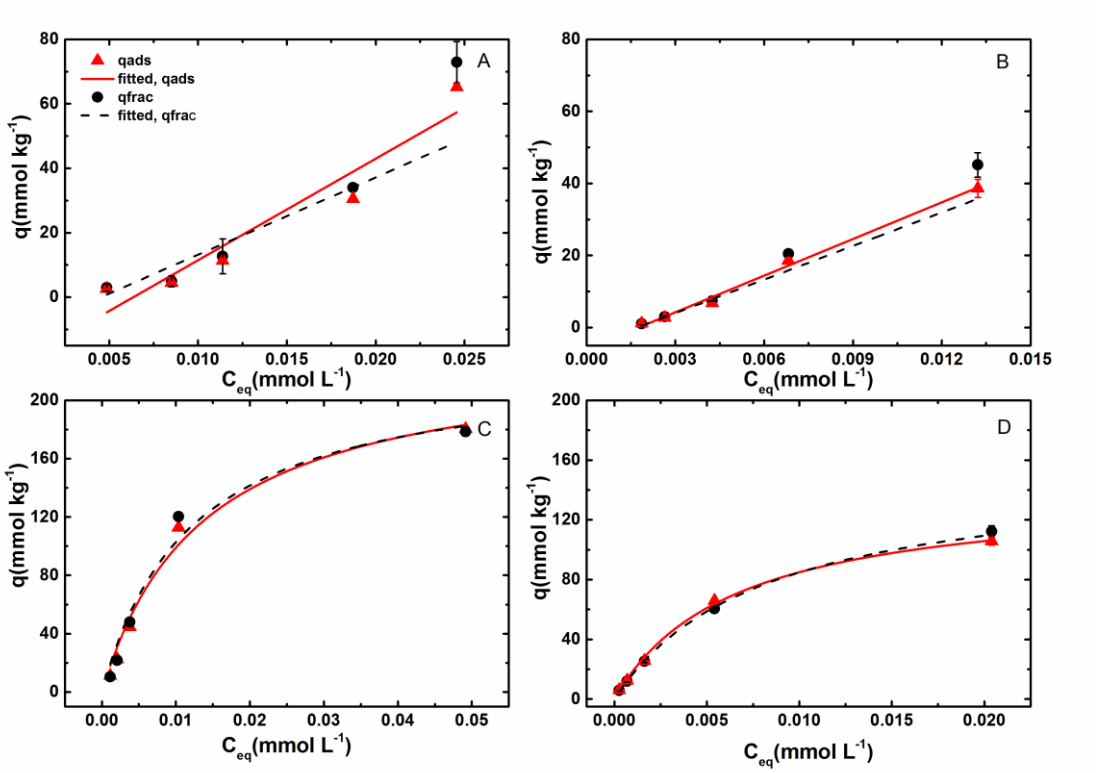

588

589

590 **Figure 1**. Sorption isotherms of Cu and Cd for low metal to biomass ratio (2g·L^{-1} *E.coli-*

591 *JM109*) and high metal to biomass ratio (0.5g ·L^{-1} *E.coli JM109*) suspensions,

592 comparing amounts adsorbed from bulk solution (qabs) with amounts adsorbed as

593 calculated from mass balance of fractionated amounts (qfrac, the sum of qexch, qperi

594 and qcyt). The points are the experiment data. The lines are the Langmuir model fits.

595 Plot A, B, C and D refer to the sorption isotherm of Cu with 2g·L^{-1} cells, Cd with 2g·L^{-}

596 ^{1} cells, Cu with 0.5 g·L^{-1} cells and Cd with 0.5g g·L^{-1} cells respectively.

597

598

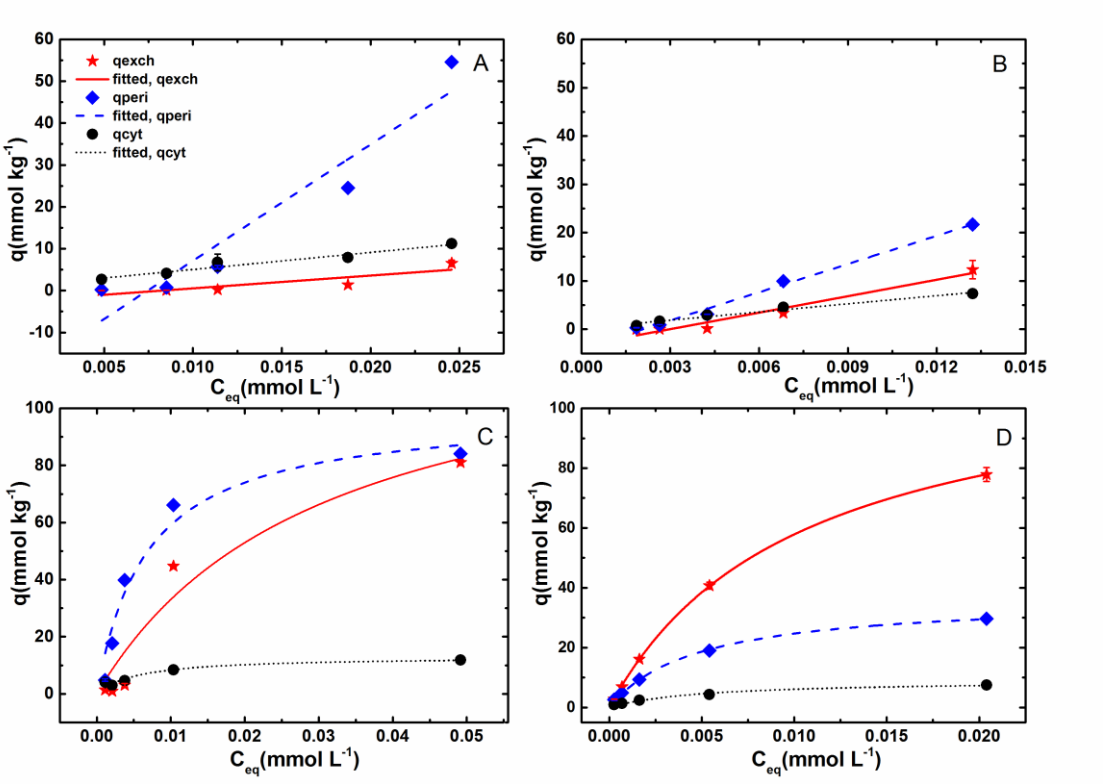

599

600

601 **Figure 2**. Sorption isotherms of Cu and Cd for low metal to biomass ratio (2g·L^{-1} *E.coli*

602 *JM109*) and high metal to biomass ratio (0.5g ·L^{-1} *E.coli JM109*) suspensions, showing

603 amounts fractionated following bulk adsorption associated with exchangeable sites

604 (qexch), the periplasmic space (qperi) and the cytoplasm (qcyt) of cells. Points are the

605 experiment data and lines are the Langmuir model fits. Plot A, B, C and D refer to the

606 sorption isotherm of Cu with 2g·L^{-1} cells, Cd with 2g·L^{-1} cells, Cu with 0.5 g·L^{-1} cells

607 and Cd with 0.5g g·L^{-1} cells respectively.

608

609

610

611

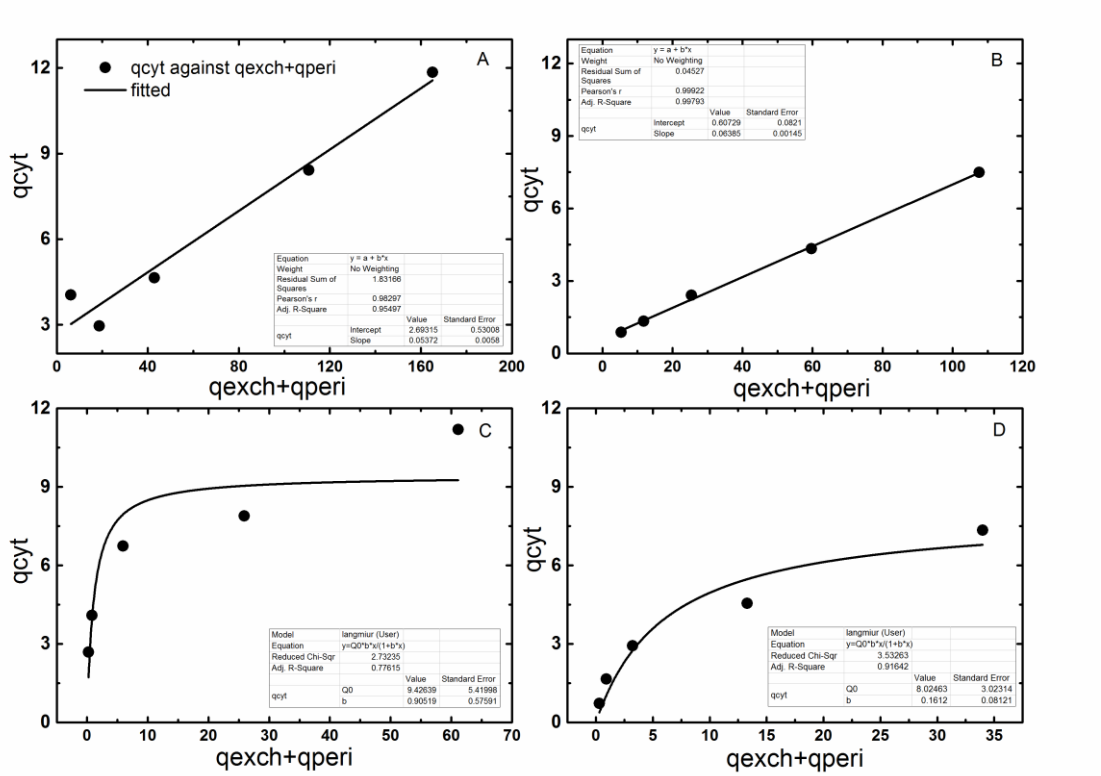

Figure 3. Graphical representation of the variation of internalised metal (qcyt) against the sum of exchangeable and periplasmic concentrations (qexch + qperi) for high metal to biomass ratios (A & B, 0.5 g·L^{-1} cells) and low metal to biomass ratio (C and D, 2g·L^{-1} cell) suspensions of Cu (left panels, A and C) and Cd (right panels, B and D). Suspensions with high metal to biomass ratios show a linear relationship, possibly representing a constant ratio between internalisation and efflux rates, consistent with equilibrium between internalised and surface-bound metals (qexch + qperi). Systems with low metal to biomass ratios start with high internalisation rates, which decreases as metal concentrations become toxic and efflux.

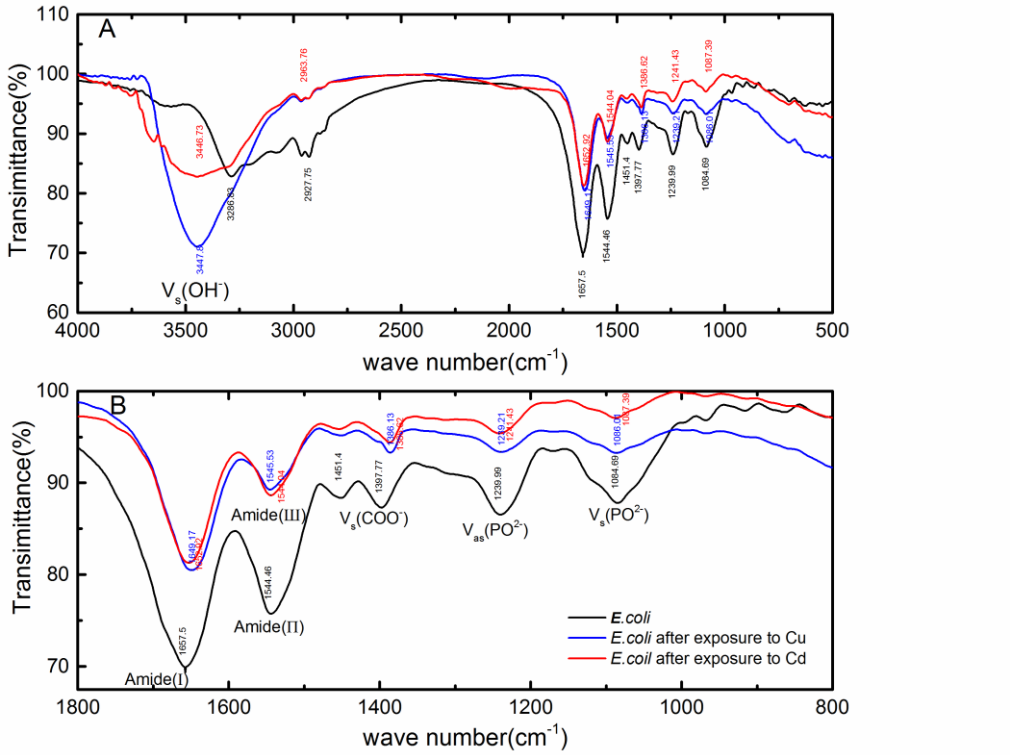

625

626

627 **Figure 4**. FTIR spectra of *E.coli* JM109 before and after exposure to Cu and Cd

628 solutions. The concentration of Cu and Cd both are 5mg/L, background is 0.01M

629 $NaNO_3$ with pH 5, and using 0.5g $\cdot L^{-1}$ bacterial suspension. The black lines refer to

630 *E.coli* without metal adsorption, blue lines and red lines refer to *E.coli* after exposure

631 to Cu and Cd solutions respectively. Plot A is the full spectrum whereas plot B focuses

632 on the bacterial fingerprint region.

633

634

635

636

637

638 **Table 1.** Langmuir parameters(Q and b) and linear parameters (Intercept and Slope),
639 which associated with surface(qexch), periplasmic space(qperi) and cytoplasm(qcyt),
640 for exposure 0.5g·L^{-1} and 2 g·L^{-1} *E.coli JM109* to Cu solution respectively.

641

Compartment	Q0 (mmol·kg-1)	b (L·kg-1)	Residual Sum of Squares	R^2	Percent of total Cu associated with each compartment of cell based on Q values(%)
Cu with 0.5g/L *E.coli-JM109*					
qexch*	134	33.0	325.8	0.916	54.3
qperi*	99.8	147.8	184.2	0.943	40.4
qcyt*	13.1	178.7	4.20	0.897	5.3
qads#	234	73.10	301.0	0.980	
qfrac#	228	82.10	506.8	0.967	
Cu with 2g/L *E.coli-JM109*					
Compartment	Intercept	Slope	R2		
qexch*	0.97	408.0	0.94		
qperi*	-20.6	2779	0.89		
qcyt*	-2.52	305.6	0.68		
qads#	-20.0	3148	0.90		
qfrac#	-10.8	2400	0.96		

642 Note: the date of * are associated with Figure 2; the date of # are associated with Figure 1.

643

644 **Table 2.** Langmuir parameters(Q and b) and linear parameters (Intercept and Slope),
645 which associated with surface(qexch), periplasmic space(qperi) and cytoplasm(qcyt),
646 for exposure 0.5g·L^{-1} and 2 g·L^{-1} *E.coli JM109* to Cd solution respectively.

647

Compartment	Q0 (mmol·kg-1)	b (L·kg-1)	Residual Sum of Squares	R^2	Percent of total Cu associated with each compartment of cell based on Q values(%)
0.5g/L E.coli JM109 exposure to Cd					
qexch*	117	97.82	0.39	1.00	71.98
qperi*	36.4	210.7	0.66	1.00	22.38
qcyt*	9.2	197.6	0.43	0.98	5.64
qads#	140	153.7	12.42	1.00	
qfrac#	154	123.4	6.90	1.00	
2g/L E.coli JM109 exposure to Cd					
Compartment	Intercept	Slope	R2		
qcyt*	0.21	562.0	0.96		
qperi*	-4.02	1947	0.99		
qexch*	-3.38	1136	0.94		
qads#	-5.93	3391	0.99		
qfrac#	-5.31	3106	0.92		

648 Note: the date of * are associated with Figure 2; the date of # are associated with Figure 1.

649

650

651

652

653

654

655 **Table 3**. Dissociation constants (p*K*a where a= 1-4) and site density (SD) in mol g^{-1} dry

656 weight/ 10^{-4} for each site on the cells of *E. coli JM109* as determined by potentiometric

657 titrations and FITEQL4 modelling. SD_T is the sum of the site concentrations.

Strain	pK1	SD	pk2	SD	pK3	SD	pK4	SD	SD_T	V(Y)
JM109	3.48	6.25	5.47	4.39	7.34	1.56	9.97	3.86	16.06	8.68

658

659